

Helicity in Large-Scale Dynamo Simulations

Axel Brandenburg

Department of Mathematics, University of Newcastle upon Tyne, NE1 7RU, UK

Various hydromagnetic turbulence simulations exhibiting large scale dynamo action are analysed: rotating convection with shear, rotating shear flow, and isotropically forced helical turbulence. The signs and magnitudes of the various helicities are compared and related to the effective dynamo alpha parameter. In isotropically forced helical flows the alpha parameter is found to be a negative multiple of the residual helicity, which is the difference between kinetic and current helicity. The convection simulations are consistent with this, but the rotating shear flow simulations are not. In the latter case shear is responsible for reversing the sign of the stress, and it is the sign of the magnetic stress that determines the sign of the magnetically driven dynamo alpha. Finally, the inverse magnetic cascade is related to the alpha effect and attempts are shown to evaluate the magnitudes of alpha and turbulent diffusivity in a simulation exhibiting an inverse cascade.

1. INTRODUCTION

The concept of helicity is central to all theories of large scale dynamos. In the early work by Parker (1955) the concept of cyclonic convection was introduced as a means of producing poloidal magnetic field from a toroidal field by twisting rising flux tubes via the Coriolis force. This was later quantified with the development of the α -effect (Steenbeck, Krause & Rädler 1966), which measures the magnitude of the mean electromotive force in the direction of the mean magnetic field. The books by Moffatt (1978) and Krause & Rädler (1980) give a comprehensive account of the kinematic mean-field dynamo theory. The main result is that when α is large enough a dynamo instability sets in and a large scale magnetic field is generated. For isotropic

turbulence the α parameter is a negative multiple of the kinetic helicity.

An important discovery was made by Frisch et al. (1975) and Pouquet et al. (1976), who found that the presence of magnetic helicity can give rise to an inverse cascade, by which magnetic helicity and energy are being transferred from small to large scales. The growth of the large scale field depends here on the *residual* helicity, i.e. the difference between kinetic and (electric) current helicities. The involvement of magnetic fields, or rather magnetically driven fluid motions, could be crucial, especially in those circumstances where the magnetic field is strong. This is the case in practically *all* astrophysically interesting applications (stars, accretion discs, and galaxies).

There are now many different simulations displaying large scale dynamo action in astrophysically relevant systems. The purpose of this paper is to compare the helicities in some of those simulations. We begin with recent simulations of overshooting convection with imposed shear. We then discuss simulations without convection and just shear, relevant to accretion discs, and finally compare with simulations of isotropically forced flows.

2. DYNAMOS FROM OVERSHOOTING CONVECTION WITH SHEAR

The overshoot layer beneath the solar convection zone proper is often thought to be the place where the dynamo operates. This is the main reason why it is useful to include overshoot in convective dynamo simulations. Results of Nordlund et al. (1992) and Brandenburg et al. (1996) suggest that dynamo action occurs actually throughout the entire convection zone proper, but that the field is then transported downwards into the overshoot layer by turbulent pumping of magnetic fields via rapidly spinning downdrafts. Recently, those simulations have been extended to include the effects of shear (Brandenburg et al. 1999). Shear takes the role of the omega-effect, although here the concept of alpha-omega dynamos is not explicitly invoked. The main result is the generation of large scale fields on the scale of the box. Those fields are of significant strength and can exceed the equipartition field strength by an order of magnitude.

For orientation we give the basic parameters of the simulation. The simulation is carried out at 30° northern latitude and the resulting inverse Rossby number, $2\Omega L/u_{\text{rms}}$, is around 5. Here, u_{rms} is the turbulent rms velocity, L is the depth of the unstable layer, and Ω is the angular velocity. Uniform latitudinal shear is imposed by a body force throughout the convection zone proper, but it vanishes towards the radiative interior, resulting in vertical shear around the lower overshoot layer. ‘Sliding-periodic’ boundary conditions (Hawley et al. 1995) are used in the cross-stream direction and ordinary periodic boundary conditions in the streamwise direction. The ratio between shear gradient and angular velocity is 0.5 and the velocity difference across the box is $\Delta U \approx \pm 0.4u_{\text{rms}}$. The resolution is $63 \times 63 \times 64$ meshpoints, the ordinary and magnetic Prandtl numbers are $\text{Pr} = \nu/\chi = 0.2$ and $\text{Pr}_M = \nu/\eta = 0.5$, i.e. the kinematic viscosity ν is smaller than the magnetic and thermal diffusivities (η and χ). In the sun the two Prandtl numbers are much smaller than unity, but this is impossible to simulate in a simulation of only modest resolution. The Reynolds number is $\text{Re} = u_{\text{rms}}L/\nu = 240$, the Rayleigh and Taylor numbers are $\text{Ra} = gL^4 s'_0/(c_p \chi \nu) = 5 \times 10^5$ and $\text{Ta} = (2\Omega L^2/\nu) = 10^6$. Here, g is gravity and s'_0 is the entropy gradient of the associated unstable hydrostatic solution.

The orientation of the cartesian box is as follows: x points north, y points east in the toroidal direction, and z points downwards. The top and bottom boundaries are stress free and the horizontal field vanishes, so there

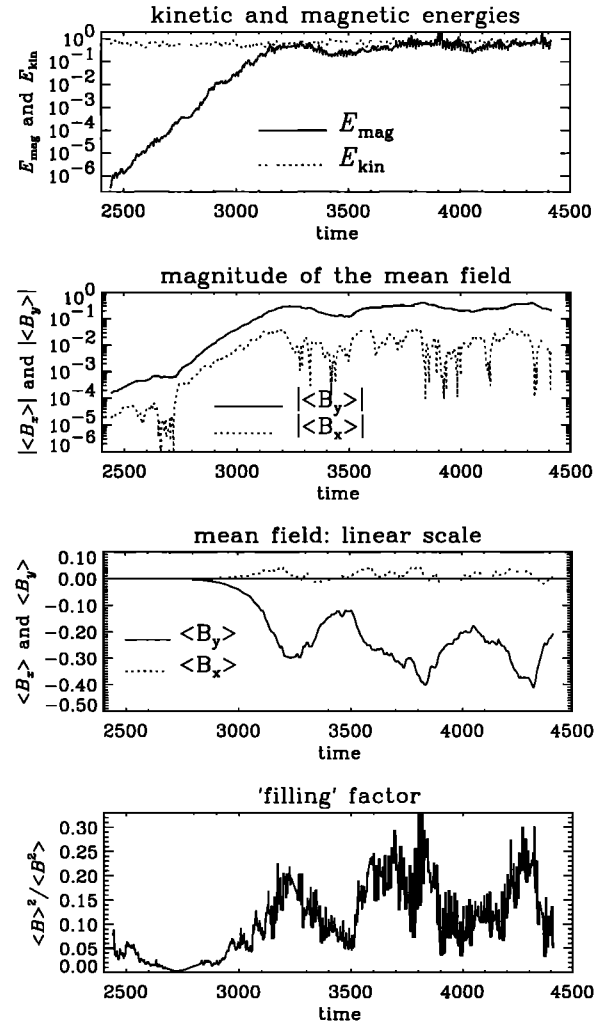


Figure 1. Evolution of magnetic and kinetic energies, mean magnetic field, and $\langle B \rangle^2 / \langle B^2 \rangle$ (which may be interpreted as a ‘filling’ factor) in a convection simulation with imposed shear.

is no vertical Poynting flux through the boundaries. Initially there is no net flux through the box.

In figure 1 we show the evolution of the total magnetic energy and the mean magnetic field in such a simulation. The magnetic energy increases by 6 orders of magnitude and then saturates. There is also an exponential growth of the *mean* field (averaged over the entire box), which increases by 3 orders of magnitude until saturation is reached. (This is at around $t = 3200$, approximately the same time when the magnetic energy saturates; the time unit is $\sqrt{L/g}$.) Note that the energy in the mean magnetic field can be as large as 20% of the total magnetic energy.

The main effect of the shear is the generation of strong ordered toroidal fields, $\langle B_y \rangle$. There is also a much weaker poloidal field component. The component in the latitudinal direction, $\langle B_x \rangle$, is about 10 times weaker and oriented mostly in the opposite direction, i.e. $\langle B_x \rangle \langle B_y \rangle < 0$ for most of the time. This is simply a consequence of the shear, $\partial U_y / \partial x < 0$, which turns a positive $\langle B_x \rangle$ into a negative $\langle B_y \rangle$.

In figure 2 we show the evolution of the various helicities for this run: kinetic helicity $\langle \boldsymbol{\omega} \cdot \mathbf{u} \rangle$, current helicity $\langle \mathbf{J} \cdot \mathbf{B} \rangle$, cross helicity $\langle \mathbf{u} \cdot \mathbf{B} \rangle$, and the magnetic helicity, $\langle \mathbf{A} \cdot \mathbf{B} \rangle$. Here, $\boldsymbol{\omega} = \text{curl } \mathbf{u}$ is the vorticity, \mathbf{u} the velocity, $\mathbf{J} = \text{curl } \mathbf{B} / \mu_0$ the current density, $\mathbf{B} = \text{curl } \mathbf{A}$ the magnetic field, \mathbf{A} the magnetic vector potential, and μ_0 the vacuum permeability.

We find that the kinetic helicity is negative, and that its magnitude *increases* as the dynamo becomes saturated, i.e. when the magnetic energy levels off. This suggests that not only the current helicity, but also the kinetic helicity is driven (at least partly) by the magnetic field. In other words, the part of the velocity that contributes mostly to the helicity integral is caused mainly by the Lorentz force. Note also that current and kinetic helicities have the *same* sign. This is in contrast to some simulations of magnetoconvection with imposed magnetic field and at smaller magnetic Reynolds number (Brandenburg et al. 1990), where the two helicities have opposite sign. This may hint at an important difference between more-or-less passive magnetic field evolution on the one hand and dynamo-generated magnetic fields on the other.

Looking at the third panel of figure 2 we note that there is also some cross helicity being generated. The cross helicity, which is perhaps more sensibly written as $\langle \mathbf{B} \cdot \text{curl}^{-1} \boldsymbol{\omega} \rangle$, measures the linkage between \mathbf{B} -tubes and $\boldsymbol{\omega}$ -tubes. Here, $\text{curl}^{-1} \boldsymbol{\omega} = \mathbf{u}$. Significant magnetic helicity, $\langle \mathbf{B} \cdot \text{curl}^{-1} \mathbf{B} \rangle$, which measures the linkage of \mathbf{B} -tubes with themselves, is also being generated at the time when the large scale field reaches saturation. That too is negative, so all three fields, $\boldsymbol{\omega}$, \mathbf{J} and \mathbf{B} , have the same sign of the linkage number after the time the large scale field saturates. Only the linkage between $\boldsymbol{\omega}$ and \mathbf{B} tubes has the opposite sign.

The helicities given in figure 2 are all calculated using the full velocity and magnetic fields. In mean-field dynamo theory one often needs the helicity calculated with respect to the fluctuations about the mean value, i.e. $\langle \boldsymbol{\omega}' \cdot \mathbf{u}' \rangle = \langle \boldsymbol{\omega} \cdot \mathbf{u} \rangle - \langle \boldsymbol{\omega} \rangle \cdot \langle \mathbf{u} \rangle$ and $\langle \mathbf{J}' \cdot \mathbf{B}' \rangle = \langle \mathbf{J} \cdot \mathbf{B} \rangle - \langle \mathbf{J} \rangle \cdot \langle \mathbf{B} \rangle$. The difference is negligible, however, because the large scale kinetic and current helicities are small; see the dotted lines in figure 2a and

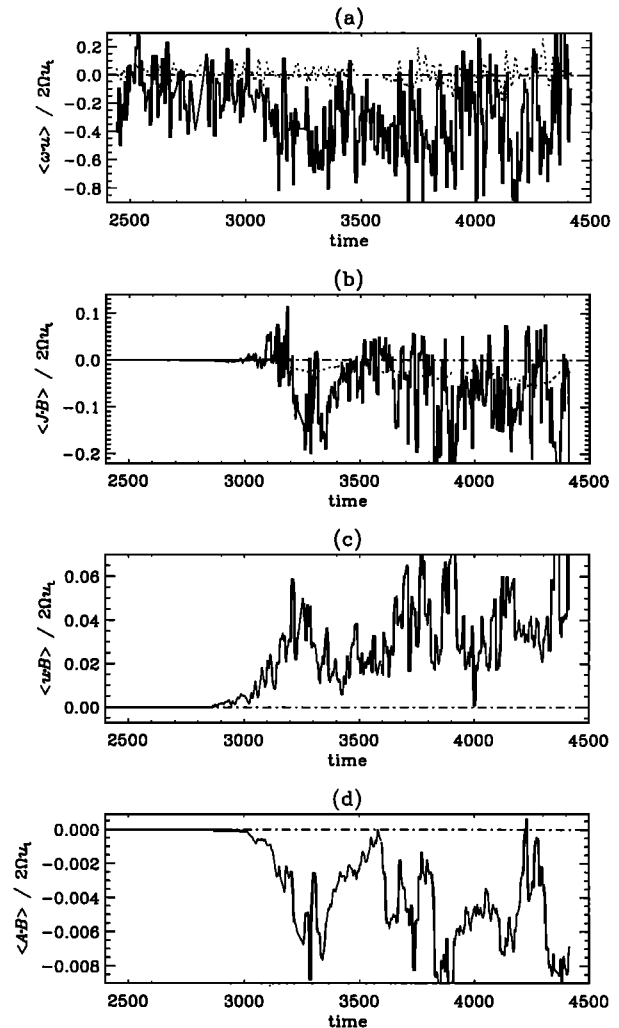


Figure 2. Evolution of kinetic helicity, current helicity, cross helicity, and magnetic helicity, in a convection simulation with imposed shear. The dotted lines in (a) and (b) give the large scale kinetic and current helicities, multiplied by a factor of 10.

b. The fluctuations in the toroidal component of the electromotive force, $\langle \mathbf{u}' \times \mathbf{B}' \rangle_y$, are large, and there is only a very weak positive correlation with the mean toroidal magnetic field, $\langle B_y \rangle$. Such a correlation would be suggestive of a positive (but very noisy) alpha-effect, if $\langle \mathbf{u}' \times \mathbf{B}' \rangle_y = \alpha_{yy} \langle B_y \rangle + \text{other terms}$. It may be surprising or even implausible that a very noisy effect could explain a strong and well-defined mean magnetic field as seen in figure 1. The reason is perhaps that even a very noisy or an incoherent alpha-effect (Vishniac & Brandenburg 1997; see also Vishniac's chapter) could give rise to a large scale magnetic field.

3. HELICITY IN SHEAR-DRIVEN ACCRETION DISC DYNAMOS

A somewhat different situation is encountered in accretion discs, where there is no direct source of turbulence, because discs are hydrodynamically stable. Only in the presence of a magnetic field there is a linear instability (Velikhov 1959, Chandrasekhar 1960, 1961). This instability is now often called the magnetorotational or Balbus-Hawley (1991) instability. However, the flows generated by this instability would tend to destroy the magnetic field via turbulent diffusion. Nevertheless, at the same time the turbulence can also amplify the magnetic field via dynamo action. Simulations unanimously point towards the possibility of a cycle where the field generates turbulence and the turbulence generates more magnetic fields (Brandenburg et al. 1995, Hawley et al. 1996, Stone et al. 1996). In particular, in simulations of Brandenburg et al. (1995) there is a large scale magnetic field, which is oscillatory and varies on a time scale of about 30 orbits, $T_{\text{rot}} = 2\pi/\Omega_0$, where Ω_0 is the angular velocity. Many quantities vary cyclically with the mean field, of which the toroidal component (B_y) is the strongest.

In figure 3 we plot the kinetic and current helicities in the upper disc plane as functions of the mean toroidal field, $\langle B_y \rangle$. Note that $\langle \mathbf{J} \cdot \mathbf{B} \rangle$ is approximately proportional to $\langle B_y \rangle^2$, as indicated by the solid line. On the other hand, $\langle \boldsymbol{\omega} \cdot \mathbf{u} \rangle$ shows strong scatter and is independent of $\langle B_y \rangle$. In contrast to the case of convection with shear the kinetic and current helicities have now opposite signs. The negative sign of $\langle \boldsymbol{\omega} \cdot \mathbf{u} \rangle$ is in agreement with the interpretation in terms of cyclonic motions, but the sign of $\langle \mathbf{J} \cdot \mathbf{B} \rangle$ is not. At large scales the signs of the two helicities are actually different (see the lower two panels of figure 3), but their magnitudes are small, so this does not explain the result. So, the origin of the sign of $\langle \mathbf{J} \cdot \mathbf{B} \rangle$ remains unclear. It is probably connected with the strong effects of shear, which can give rise to unusual signs of the α -effect. This will be discussed next. The connection between α and $\langle \mathbf{J} \cdot \mathbf{B} \rangle$ will be discussed in the following section.

In the case of the accretion disc simulations it is possible to estimate the magnitude and sign of the effective dynamo α parameter by correlating at different time steps the mean electromotive force with the resulting mean magnetic field and to establish a fit of the form $\langle \mathbf{u}' \times \mathbf{B}' \rangle_y = \alpha \langle B_y \rangle$ (Brandenburg et al. 1995, Brandenburg & Donner 1997). Here primes denote fluctuations. The α measured in that way is found to be *negative* in the upper disc plane. Therefore, the sign of α is in

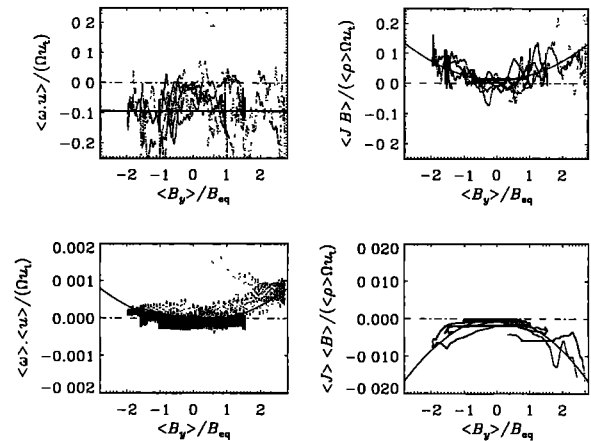


Figure 3. Kinetic helicity and current helicity in the upper disc plane of in an accretion disc dynamo simulation. The lines give a fit through the data. The last two panels show that the two helicities of the mean field are small and of opposite sign.

disagreement with that expected from kinetic and current helicities (see the next section). The perhaps most convincing explanation for this negative sign is that the shear twists buoyant magnetic structures in the opposite sense as the Coriolis force (Brandenburg & Campbell 1997, Brandenburg 1997, 1998, 1999). The mean toroidal electromagnetic force, $\langle \mathbf{u}' \times \mathbf{B}' \rangle_y$, is then governed by the vertical velocity fluctuations u'_z , and radial magnetic field fluctuations, B'_x , so $\langle \mathbf{u}' \times \mathbf{B}' \rangle_y = \langle u'_z B'_x \rangle$. If u'_z originates mainly from magnetic buoyancy then $u'_z \sim -(\rho'/\langle \rho \rangle)g\tau$, where τ is some relevant timescale and $\rho'/\langle \rho \rangle \approx \langle B_y \rangle B'_y / \langle \mu_0 \rho c_s^2 \rangle$, so $\langle \mathbf{u}' \times \mathbf{B}' \rangle_y = \alpha \langle B_y \rangle$ with $\alpha \sim \langle B'_x B'_y \rangle g\tau / \langle \mu_0 \rho c_s^2 \rangle$. This would explain the negative sign of α , because $\langle B_x B_y \rangle < 0$ (in agreement with the sign of the mean shear, $\partial U_y / \partial x = -\frac{3}{2}\Omega_0$). This is an example where a negative α results from a flow that is driven exclusively by the Lorentz force and not, like in the case of convection, by thermal buoyancy of other nonmagnetic forces.

4. THE RELATION BETWEEN ALPHA-EFFECT AND HELICITY

There have been attempts to estimate α from forced MHD turbulence. Simulations of Tao et al. (1993), for example, verify that α is a negative multiple of the kinetic helicity. However, there has so far been no verification that α is related to the *residual* helicity (Pouquet et al. 1976),

$$H_{\text{res}} = \langle \boldsymbol{\omega} \cdot \mathbf{u} \rangle - \langle \mathbf{J} \cdot \mathbf{B} \rangle / \rho. \quad (1)$$

The $\langle \mathbf{J} \cdot \mathbf{B} \rangle$ term in this expression can lead to significant modifications once the magnetic energy is strong compared with the kinetic energy. This is likely to be case in accretion discs. In order to access this parameter regime we now discuss another model (Brandenburg & Bigazzi 1999) where the flow is magnetically driven. In that case we adopt some random forcing, \mathbf{E}_f , directly in the induction equation, which then takes the form

$$\frac{\partial \mathbf{A}}{\partial t} = \mathbf{u} \times \mathbf{B} + \eta \nabla^2 \mathbf{A} - \mathbf{E}_f, \quad (2)$$

where \mathbf{E}_f consists of plane Beltrami waves of maximum (positive) helicity. The spatial pattern is renewed in regular time intervals, Δt_f .

An explicit forcing in the induction equation is adopted mainly for mathematical convenience, rather than physical reality. In the case of accretion discs there is actually an extra term, $\mathbf{E}_f = SA_y \hat{x}$, where S is the shear parameter, but this corresponds to a multiplicative forcing, not to an additive forcing as in the present model, because \mathbf{E}_f is proportional to the y -component of \mathbf{A} . We comment further on this forcing term in the next section, where we adopt a forcing at high wavenumbers.

In the present model a large scale vertical magnetic field is imposed, so the field in Eq. (2) consists of two parts: $\mathbf{B} = \hat{z}B_0 + \nabla \times \mathbf{A}$. The flow is driven exclusively by the Lorentz force in the momentum equation. The resulting current helicity is large and positive, and the kinetic helicity has now the *same* sign, i.e. $\langle \boldsymbol{\omega} \cdot \mathbf{u} \rangle > 0$ and $\langle \mathbf{J} \cdot \mathbf{B} \rangle > 0$, but with $|\langle \boldsymbol{\omega} \cdot \mathbf{u} \rangle| \ll |\langle \mathbf{J} \cdot \mathbf{B} \rangle|$.

We measure the dynamo α by dividing the z -component of the resulting electromotive force, $\mathcal{E} = \langle \mathbf{u} \times \mathbf{B} \rangle$, by B_0 . We find that to a good approximation α is a negative multiple of H_{res} ; see figure 4. In the present case with magnetic forcing the residual helicity is always negative, because the current helicity dominates over the kinetic helicity and both are positive. A somewhat different situation arises when the forcing is applied in the momentum equation instead. In that case the kinetic helicity is larger than the current helicity and so the sign of the residual helicity is positive. The corresponding sign of α is then also reversed. This is how we obtained the points on the right hand side of figure 4 for positive values of H_{res} . The data points for both magnetic and hydrodynamic forcing match the linear fit equally well.

Although the approach in this section is enlightening as far as the connection between α and the various helicities is concerned, it remains unsatisfactory for a number of reasons. Firstly, for small imposed fields and sufficiently large magnetic Reynolds numbers there is a dynamo effect that causes the mean electromotive

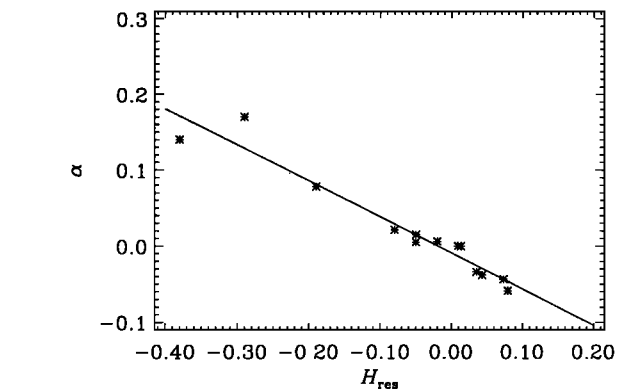


Figure 4. Alpha effect as a function of residual helicity.

force to grow to large values until saturation occurs. At the same time the mean magnetic field is conserved. Thus there can be no casual relation between the mean electromotive force and the mean magnetic field. It is therefore no longer possible to estimate α by just dividing the electromotive force by B_0 . The result would have been arbitrary and therefore meaningless. This difficulty does not arise for small magnetic Reynolds numbers, although that case is of course less interesting. Secondly, when measuring α using averages defined by projections onto the $k = 0$ wavenumber the results may be spurious, because the field in the $k = 0$ wavenumber (i.e. the flux through the box) is conserved for periodic boundary conditions and therefore not affected by the dynamics. A more satisfactory approach is therefore to measure α by projecting onto the wavenumber $k = 1$ and forcing at sufficiently small scale to have some sort of scale separation. This is done in the next section. One could still use an initial field at wavenumber $k = 1$, but now this field can evolve. We find that it grows to appreciable field strengths due to dynamo action, and it is such a state that will be used for estimating α . First, however, we look at the growth of the field starting from random initial conditions.

5. THE INVERSE CASCADE EFFECT IN ISOTROPICALLY FORCED SYSTEMS

Following the early work on inverse cascades (Pouquet et al. 1976) we now adopt a *high* wavenumber forcing in the induction equation. Apart from the higher forcing wavenumber and the absence of an imposed field everything else is like in the previous section. Because the forcing is at high wavenumbers only ($k = 10$) the magnetic field evolution at the large scales ($k = 1$) is not immediately affected, except of course for the inverse

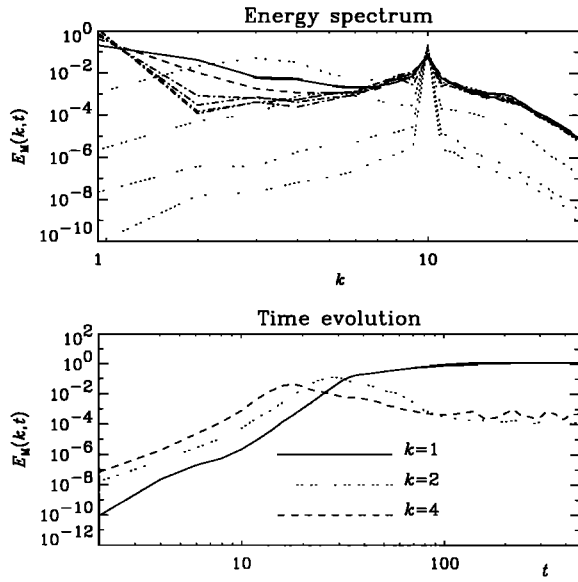


Figure 5. The inverse cascade seen in power spectra of the magnetic field taken at different times (upper panel). The four dotted curves are for $t = 2, 4, 10, 20$, the solid and dashed curves are for $t = 40$ and 60 , respectively, and the dash-dotted curves are for $t = 80, 100, 200$, and 400 . The lower panel shows the evolution of the spectral power in the $k = 1, 2$, and 4 modes in a double-logarithmic plot.

cascade effect which governs the evolution on wavenumbers smaller than the forcing wavenumber. We also point out that the general behavior is similar, regardless of whether the forcing is applied in the induction equation or in the momentum equation.

Looking at power spectra of the magnetic field at subsequent times (figure 5) we see that the energy at the largest possible scale in the system ($k = 1$) grows until some saturation level is reached at around $t = 40$; see the lower panel of figure 5. Curiously enough, at the time when the $k = 1$ mode reaches saturation the power in the $k = 2$ mode begins to be suppressed (see the dotted line). Looking more carefully at this plot reveals that at the time when the $k = 2$ mode began to saturate (at around $t = 20 - 30$) the power in the next higher modes, $k = 3$ and $k = 4$, was suppressed. This has also been observed in similar calculations of low Reynolds number flows (Gilbert & Sulem 1990, Galanti et al. 1991, Galanti & Sulem 1991). In our case the Reynolds numbers (ordinary and magnetic), based on the box size and the rms velocity, are around 140. However, the Reynolds number based on the wavenumber 10 is only 14. In that sense our simulation too is rather diffusive.

The orientation of the magnetic field is not determined a priori and depends on chance and on initial conditions. Sometimes we found a field that varied mostly in the x -direction, while for other simulations the field varied mostly in the y or z -directions. If the mean field varies only in the x -direction, for example, then $\partial_y \langle \mathbf{B} \rangle = \partial_z \langle \mathbf{B} \rangle = 0$ and only $\partial_x \langle \mathbf{B} \rangle$ is nontrivial. Then, however, because

$$0 = \nabla \cdot \langle \mathbf{B} \rangle = \partial_x \langle B_x \rangle, \quad (3)$$

we have $\langle B_x \rangle = \text{const} = 0$, so $\langle \mathbf{B} \rangle = (0, \langle B_y \rangle, \langle B_z \rangle)$. In other words, the field vector lies in a plane whose normal is parallel to the direction in which it varies, but it has no component in that direction. Once the large scale field has selected a preferred direction, it will stick to it for all times. We note, however, that we never encountered a case where the field is oblique to any of the coordinate planes. An oblique mean field would diffuse faster, because the turbulent diffusion operator, $\eta_t(k_x^2 + k_y^2) = 2\eta_t k_{\min}^2$, is always larger than just $\eta_t k_x^2 = \eta_t k_{\min}^2$. This is probably the reason why diagonal fields are not being generated.

In figure 6 we show the resulting mean magnetic field from a simulation in which the preferred direction of the mean field is the z -direction. Note that there is a 90° phase difference between the x and y -components of the mean magnetic field.

The approach just described allows us to study the evolution and saturation of the large scale magnetic field. An obvious question is then whether the field produced by the inverse cascade resembles qualitatively and perhaps even quantitatively the field generated by an α^2 dynamo, and if so, what are then the corresponding values of α and turbulent diffusivity, η_t .

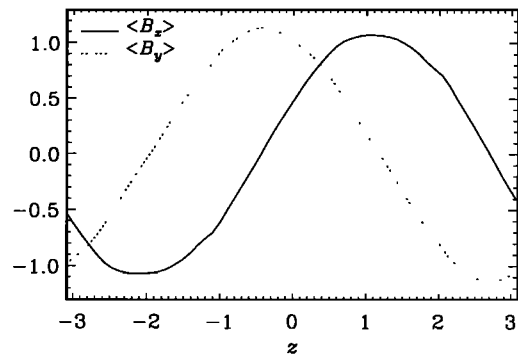


Figure 6. The mean magnetic field components, $\langle B_x \rangle$ and $\langle B_y \rangle$, as functions of z in a simulation where the mean field varies only in the z -direction.

6. CONNECTION WITH AN ALPHA-SQUARED DYNAMO

The mean magnetic field found in the previous section resembles in many ways an α^2 dynamo. In such a dynamo the large scale field is governed by the equations

$$\frac{\partial \langle B_x \rangle}{\partial t} = -\alpha \frac{\partial \langle B_y \rangle}{\partial z} + (\eta + \eta_t) \frac{\partial^2 \langle B_x \rangle}{\partial z^2}, \quad (4)$$

$$\frac{\partial \langle B_y \rangle}{\partial t} = +\alpha \frac{\partial \langle B_x \rangle}{\partial z} + (\eta + \eta_t) \frac{\partial^2 \langle B_y \rangle}{\partial z^2}, \quad (5)$$

where we have assumed that the mean field varies only in the z -direction, which is the situation in the particular solution displayed in figure 6 (section 5). The averages are taken over the x and y directions. In the saturated case the field is dominated by the smallest wavenumber $k = 1$; see the inset of figure 5. Therefore we now take the solution to be of the form

$$\langle B_x \rangle = \hat{B}_x(t) \sin(z - z_0), \quad \langle B_y \rangle = \hat{B}_y(t) \cos(z - z_0), \quad (6)$$

where z_0 is a constant (phase factor). With this, Eqs. (4) and (5) take the form

$$\frac{\partial \hat{B}_x}{\partial t} = \alpha \hat{B}_y - (\eta + \eta_t) \hat{B}_x, \quad (7)$$

$$\frac{\partial \hat{B}_y}{\partial t} = \alpha \hat{B}_x - (\eta + \eta_t) \hat{B}_y. \quad (8)$$

In the steady state we have $\alpha = \eta + \eta_t$. In order to estimate the value of α we modify the actual field in the simulation by setting momentarily the mean field in either the x or the y -direction to zero, i.e. we replace at some instance in time $B_x \rightarrow B_x - \langle B_x \rangle$ or $B_y \rightarrow B_y - \langle B_y \rangle$. Looking at eq. (7) we see that setting $\langle B_x \rangle = \hat{B}_x = 0$ means that immediately after this manipulation the \hat{B}_x field should recover at a rate $\alpha \hat{B}_y$. This rate is approximately 0.02 (see figure 7), and since $\hat{B}_y \approx 1$ we have $\alpha \approx 0.02$. This value is already affected by the nonlinear feedback in the system (alpha-quenching, for example). Assuming that the value of α is the same before and after removing one of the two mean field components we have therefore $\eta + \eta_t \approx \alpha \approx 0.02$. Since in this simulation $\eta = 0.01$ we have $\eta_t \approx \eta$. Those values of α and η_t are rather small, suggesting again that the effective magnetic Reynolds number is small.

This method can in principle be applied to systems with different field strengths, different magnetic Reynolds numbers, and different amounts of helicity.

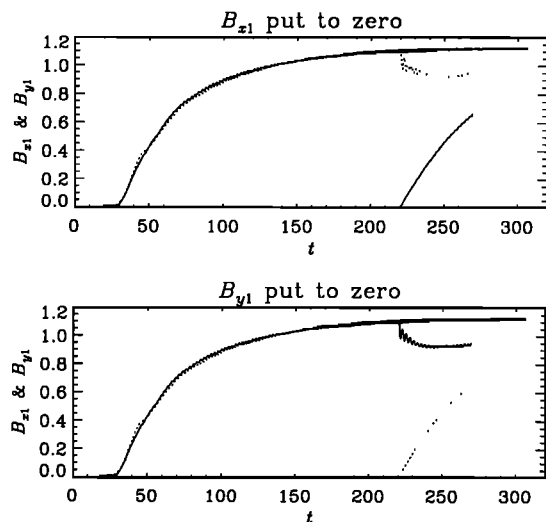


Figure 7. Response of the large scale field after removing the mean field from the B_x and B_y fields, respectively. After $t = 220$ the field component that was set to zero (\hat{B}_x in the upper panel, \hat{B}_y in the lower) began to grow at a rate ≈ 0.02 .

7. CONCLUSIONS

Helicity is closely connected with large scale dynamos. In isotropically forced turbulence helicity leads to a growth of the large scale field in a way that is very similar to the case of α -effect mean-field dynamos. Measuring the value of α in such a case gave evidence that this α is a negative multiple of the residual helicity, as was expected some time ago by Frisch et al. (1975) and Pouquet et al. (1976). However, in the non-isotropic case (sections 2 and 3) the situation is not so obvious and there may no longer be a clear relation between α and helicity, or it may be more complicated and affected by other factors such as shear, for example. Another important point is that in the inverse cascade mechanism the large scale field appears to saturate by quenching the power in the next higher Fourier modes. This suggests that modelling this phenomenon in terms of the α -effect requires some modification such as a k -dependence of α in Fourier space. However, a multiplication of the form $\alpha(k)\hat{B}(k)$ corresponds, in real space, to a convolution with some α -kernel. Such possibilities were recently explored by Brandenburg and Sokoloff (1999), and may even be necessary to explain stellar cycle data (Brandenburg et al. 1998).

Looking at figure 5 we note that once the field has reached saturation at some wavenumber, the power in the next larger wavenumber begins to be suppressed.

This may be interpreted in terms of a wavenumber dependent quenching. However, only future work can show whether the apparent similarity with α -effect dynamos is coincidental or not. Whatever the result is, it is clear that in both approaches (inverse cascade and α -effect) helicity does play an important role.

There is another important issue that needs to be mentioned here. In all situations of practical relevance the relative kinetic and current helicities (normalized by the rms values of velocity and vorticity or magnetic field and current, respectively) are never close to 100%, as was the case in the cascade model. In the simulations of rotating convective and shear flow turbulence, for example, the relative helicities were at most around 3%-5%. However, it is important to realize that even for zero net helicity, and just helicity fluctuations, a large scale field can grow, provided there is shear; see Vishniac & Brandenburg (1997). The large scale field generated in such a case varies somewhat irregularly in time and may show reversals on a diffusive time scale, so this effect alone would be insufficient to explain the solar cycle, which is more regular. Nevertheless, it is quite plausible that even a small amount of net helicity suffices to produce mean fields with the spatial and temporal order seen on the sun. Therefore, when measuring the helicity in the sun observationally it is important to measure not only the mean helicity, but also its variance (see the chapter by Pevtsov, for example).

REFERENCES

- Balbus, S. A. & Hawley, J. F. 1991 A powerful local shear instability in weakly magnetized disks. I. Linear analysis. *Astrophys. J.* 376, 214-222.
- Brandenburg, A. 1997 Large scale turbulent dynamos. *Acta Astron. Geophys. Univ. Comenianae* XIX, 235-261.
- Brandenburg, A. 1998 Theoretical Basis of Stellar Activity Cycles. In *Tenth Cambridge Workshop on Cool Stars, Stellar Systems, and the Sun* (ed. R. Donahue & J. Bookbinder), pp. 173-191. Astron. Soc. Pac. Conf. Ser., Col. 154.
- Brandenburg, A. 1999 Disc Turbulence and Viscosity. In *Theory of Black Hole Accretion Discs* (ed. M. A. Abramowicz, G. Björnsson & J. E. Pringle), Cambridge University Press.
- Brandenburg, A. & Bigazzi, A. 1999 "Nonlinear alpha-effect and inverse cascade in hydromagnetic turbulence," *Astrophys. J.* (to be submitted).
- Brandenburg, A. & Campbell, C. G. 1997 Modelling magnetised accretion discs. In *Accretion disks - New aspects* (ed. H. Spruit & E. Meyer-Hofmeister), pp. 109-124. Springer-Verlag.
- Brandenburg, A. & Donner, K. J. 1997 The dependence of the dynamo alpha on vorticity. *Monthly Notices Roy. Astron. Soc.* 288, L29-L33.
- Brandenburg, A. & Sokoloff, D. 1999 "Local and nonlocal magnetic diffusion and alpha-effect tensors in shear flow turbulence," *Geophys. Astrophys. Fluid Dyn.* (submitted).
- Brandenburg, A., Nordlund, Å., Pulkkinen, P., Stein, R.F., & Tuominen, I. 1990 3-D Simulation of turbulent cyclonic magneto-convection. *Astron. Astrophys.* 232, 277-291.
- Brandenburg, A., Nordlund, Å., Stein, R. F., & Torkelsson, U. 1995 Dynamo generated turbulence and large scale magnetic fields in a Keplerian shear flow. *Astrophys. J.* 446, 741-754.
- Brandenburg, A., Jennings, R. L., Nordlund, Å., Rieutord, M., Stein, R. F., & Tuominen, I. 1996 Magnetic structures in a dynamo simulation. *J. Fluid Mech.* 306, 325-352.
- Brandenburg, A., Saar, S. H., & Turpin, C. R. 1998 Time evolution of the magnetic activity cycle period. *Astrophys. J. Letters* 498, L51-L54.
- Brandenburg, A., Nordlund, Å., & Stein, R. F. 1999 "Simulation of a convective dynamo with imposed shear," *Astron. Astrophys.* (to be submitted).
- Chandrasekhar, S. 1960 The stability of non-dissipative Couette flow in hydromagnetics. *Proc. Natl. Acad. Sci.* 46, 253-257.
- Chandrasekhar, S. 1961 *Hydrodynamic and Hydromagnetic Stability*. Dover Publications, New York., pp. 384
- Frisch, U., Pouquet, A., L  orat, J., & Mazure, A. 1975 Possibility of an inverse cascade of magnetic helicity in hydrodynamic turbulence. *J. Fluid Mech.* 68, 769-778.
- Galanti, B. & Sulem, P.-L. 1991 Inverse cascades in three-dimensional anisotropic flows lacking parity invariance. *Phys. Fluids A* 3, 1778-1784.
- Galanti, B., Sulem, P.-L. & Gilbert, A. D. 1991 Inverse cascades and time-dependent dynamos in MHD flows. *Physica D* 47, 416-426.
- Gilbert, A. D. & Sulem, P.-L. 1990 On inverse cascades in alpha effect dynamos. *Geophys. Astrophys. Fluid Dyn.* 51, 243-261.
- Hawley, J. F., Gammie, C. F., & Balbus, S. A. 1995 Local three-dimensional magnetohydrodynamic simulations of accretion discs. *Astrophys. J.* 440, 742-763.
- Hawley, J. F., Gammie, C. F., & Balbus, S. A. 1996 Local three dimensional simulations of an accretion disk hydro-magnetic dynamo. *Astrophys. J.* 464, 690-703.
- Krause, F., & R  dler, K.-H. 1980 *Mean-Field Magnetohydrodynamics and Dynamo Theory*. Akademie-Verlag, Berlin; also Pergamon Press, Oxford.
- Moffatt, H. K. 1978 *Magnetic Field Generation in Electrically Conducting Fluids*. Cambridge University Press, Cambridge.
- Nordlund, Å., Brandenburg, A., Jennings, R. L., Rieutord, M., Ruokolainen, J., Stein, R. F., & Tuominen, I. 1992 Dynamo action in stratified convection with overshoot. *Astrophys. J.* 392, 647-652.
- Parker, E. N. 1955 Hydromagnetic dynamo models. *Astrophys. J.* 122, 293-314.
- Pouquet, A., Frisch, U., & L  orat, J. 1976 Strong MHD helical turbulence and the nonlinear dynamo effect. *J. Fluid Mech.* 77, 321-354.

- Steenbeck, M., Krause, & F., Rädler, K.-H. 1966 Berechnung der mittleren Lorentz-Feldstärke $\overline{v \times \mathbf{B}}$ für ein elektrisch leitendes Medium in turbulenter, durch Coriolis-Kräfte beeinflusster Bewegung. *Z. Naturforsch.* 21a, 369-376. See also the translation in Roberts & Stix, *The turbulent dynamo...*, Tech. Note 60, NCAR, Boulder, Colorado (1971).
- Stone, J. M., Hawley, J. F., Gammie, C. F., & Balbus, S. A. 1996 Three dimensional magnetohydrodynamical simulations of vertically stratified accretion disks. *Astrophys. J.* 463, 656-669.
- Velikhov, E. P. 1959 Stability of an ideally conducting liquid flowing between cylinders rotating in a magnetic field. *Sov. Phys. JETP* 36, 1398-1404. (Vol. 9, p. 995 in English translation)
- Vishniac, E. T. & Brandenburg, A. 1997 An incoherent $\alpha - \Omega$ dynamo in accretion disks. *Astrophys. J.* 475, 263-274.

Axel Brandenburg, Department of Mathematics, University of Newcastle upon Tyne, NE1 7RU, UK (email: Axel.Brandenburg@Newcastle.ac.uk)